JACS
JOURNAL OF THE AMERICAN CHEMICAL SOCIETY

ARTICLE

pubs.acs.org/JACS

Stimulus-Responsive Self-Assembly: Reversible, Redox-Controlled Micellization of Polyferrocenylsilane Diblock Copolymers

Jean-Charles Eloi,[‡] David A. Rider,[†,§] Graeme Cambridge,[†] George R. Whittell,[‡] Mitchell A. Winnik,*[,†] and Ian Manners*[,‡]

[‡]School of Chemistry, University of Bristol, Bristol BS8 1TS, England

[†]Department of Chemistry, University of Toronto, 80 St. George Street, Toronto M5S 3H6, Ontario, Canada

Supporting Information

ABSTRACT: In depth studies of the use of electron transfer reactions as a means to control the self-assembly of diblock copolymers with an electroactive metalloblock are reported. Specifically, the redox-triggered self-assembly of a series of polystyrene-*block*-polyferrocenylsilane (PS-*b*-PFS) diblock copolymers in dichloromethane solution is described. In the case of the amorphous polystyrene$_n$-*b*-poly(ferrocenylphenylmethylsilane)$_m$ diblock copolymers (PS$_n$-*b*-PFMPS$_m$: n = 548, m = 73; n = 71, m = 165; where n and m are the number-averaged degrees of polymerization), spherical micelles with an oxidized PFS core and a PS corona were formed upon oxidation of more than 50% of the ferrocenyl units by $[N(C_6H_4Br\text{-}4)_3][SbX_6]$ (X = Cl, F). Analogous block copolymers containing a poly(ferrocenylethylmethylsilane) (PFEMS) metalloblock, which has a lower glass transition temperature, behaved similarly. However, in contrast, on replacement of the amorphous metallopolymer blocks by semicrystalline poly(ferrocenyldimethylsilane) (PFDMS) segments, a change in the observed morphology was detected with the formation of ribbon-like micelles upon oxidation of PS$_{535}$-*b*-PFDMS$_{103}$ above the same threshold value. Again the coronas consisted of fully solvated PS and the core consisted of partially to fully oxidized PFS associated with the counteranions. When oxidation was performed with $[N(C_6H_4Br\text{-}4)_3][SbF_6]$, reduction of the cores of the spherical or ribbon-like micelles with $[Co(\eta\text{-}C_5Me_5)_2]$ enabled full recovery of the neutral chains and no significant chain scission was detected.

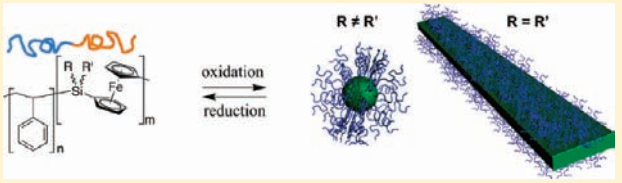

INTRODUCTION

The self-assembly of diblock copolymers in solution relies on the solubility difference between the two blocks in a given solvent. This gives rise to the formation of nanoscopic micellar aggregates with various shapes (spheres, cylinders, platelets, vesicles, etc.) where the soluble block forms the corona and the insoluble block forms a denser core.[1−9] These morphologies depend on several parameters such as the block ratio, the compositional difference in the chemistries of the blocks, the nature of the solvent, and the temperature. Typically, a small volume of a solution of diblock copolymer unimers in a good solvent for both blocks is mixed with a larger volume of a nonsolvent for one of the blocks. To disassemble the micelles, one normally adds more of the good solvent for both blocks. The ability to control the formation and disassembly of micellar aggregates has attracted intense recent attention and is of particular interest for drug delivery applications when the disassembly of the micelles (and associated drug release) needs to be triggered under special conditions.[10] Several strategies have been developed, mostly dealing with the inherent chemistry of one or both of the blocks. pH and temperature are the most commonly utilized external stimuli in terms of micelle formation.[11−15] For example, Lecommandoux et al. reported the reversible assembly-disassembly of polypeptide diblock copolymers triggered by the change in pH where both blocks acted as either corona or core depending on the acidity or alkalinity of the solution.[13] Hammond and co-workers recently reported the reversible formation of micelles of linear-dendritic polymers with response to temperature where the linear block was insoluble above its lower critical solution temperature (LCST).[14] The use of other external stimuli such as light and combinations of different stimuli have also been studied.[15−17] In contrast, redox-triggered self-assembly of block copolymers in solution is much less explored.[18−26] Most examples involve the use of atom transfer or bond reorganization redox processes to disassemble micelles. For example, Tirelli and Hubbell[19] studied the destabilization of vesicles formed with the irreversible change of the hydrophobic poly(propylene sulfide) into the more hydrophilic poly(propylene sulfone) upon oxidation. Similarly, electrochemistry was used to disrupt micelles formed from a poly(ethyleneoxide)-*b*-poly(methacrylate) copolymer containing electroactive coumarin units grafted to the latter block, as reported by Zhao et al.[20] In addition, Xu, Zhang and co-workers have described block copolymers that exhibit redox-controlled self-assembly on both oxidation and reduction.[21] Examples utilizing reversible electron transfer to control the self-assembly process are very limited and have focused on the use of electroactive tetrathiafulvalene,[22] tetraaniline,[23] ferrocene[24] and other iron compounds,[25] including redox-active anions.[26]

Received: November 24, 2010
Published: May 18, 2011

dx.doi.org/10.1021/ja1105656 | J. Am. Chem. Soc. 2011, 133, 8903–8913

Polyferrocenylsilanes (PFSs)[27−29] are versatile polymers that contain alternating iron centers and organosilicon units in the main chain. Over the past decade, these materials have been extensively studied and their redox properties associated with the reversible Fe^{II}/Fe^{III} couple are now well-understood.[30,31] For example, these polymers have been used to create photonic ink (P-Ink) devices where the swelling of a PFS gel containing silica microspheres or air-voids is controlled by the degree of oxidation of the ferrocene moieties to create colored pixelated displays.[32,33] PFS has also been used to create redox-responsive hydrogels,[34] surfaces,[35] and polyelectrolyte multilayer capsules,[36] the latter of which showed controllable permeation to fluorescent dyes. Single molecular motors, driven by the difference in elasticity between neutral and electrochemically oxidized PFS single chains, have been realized by utilizing the reversible redox properties of the material and atomic force microscopy (AFM).[37] In addition, redox-responsive PFS microspheres and microfibers, prepared by electrospinning, have also been studied.[38]

The self-assembly behavior of diblock copolymers containing a PFS segment on oxidation has been explored, but only in the solid state.[39] For example, stabilization of the disordered state in the bulk was observed upon oxidation of polystyrene-*b*-polyferrocenylsilane and polyisoprene-*b*-polyferrocenylsilane.[40] In addition, thin films of the former material have been studied using conducting probe AFM, which resolves the PFS nanodomains.[41]

In this paper, we report a detailed study[42] of the micellization and reversible disassembly of polystyrene-*b*-polyferrocenylsilane (PS-*b*-PFS) copolymers using the controllable chemical oxidation of the ferrocene moieties in the PFS block to gradually change the solubility of the organometallic block. The change from neutral Fe^{II} to cationic Fe^{III} centers is accompanied by a substantial change in polarity of the block, which would be expected to render interactions with nonpolar solvents less favorable.[43]

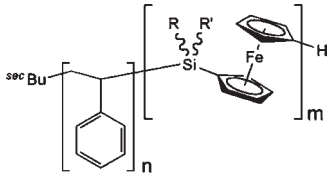

PS-*b*-PFS

RESULTS AND DISCUSSION

1. Synthesis, Oxidation, and Reduction of Organic-Organometallic Block Copolymers. PS-*b*-PFS diblock copolymers were chosen for the study since their synthesis, bulk morphology,[44,45] and the redox behavior[30,31,36] of the organometallic block have been previously well-established. Diblock copolymers with either amorphous PFS blocks [polystyrene-*b*-poly(ferrocenylmethylphenylsilane), PS-*b*-PFMPS, and polystyrene-*b*-poly(ferrocenylethylmethylsilane), PS-*b*-PFEMS, Scheme 1] or semicrystalline PFS blocks [polystyrene-*b*-poly(ferrocenyldimethylsilane), PS-*b*-PFDMS] were employed, and provided the first examples of fully reversible assembly disassembly of a block copolymer micelle using a redox stimulus. UV−visible (UV−vis) spectroscopy, dynamic light scattering (DLS), transmission and scanning electron microscopy (TEM and SEM, respectively) and atomic force microscopy were used to study these processes.

The block copolymers used in this study were prepared by sequential living anionic polymerization of styrene and the appropriately substituted sila[1]ferrocenophanes.[44] The block ratios were determined by integrating characteristic peaks of the two blocks in the ^1H NMR spectrum, and converted to volume fractions with the block densities. The molecular weights of the diblock copolymers were calculated from the absolute molecular weight of the PS block, obtained by gel permeation chromatography (GPC), and the block ratio. The polydispersity index (PDI) of the materials is reported as that determined by GPC relative to monodisperse polystyrene standards. Table 1 summarizes the diblock copolymers used in this study.

It has been previously demonstrated that $FeCl_3$[46,47a] and $[(4\text{-}BrC_6H_4)_3N][SbCl_6]$[47a] can oxidize all of the ferrocenyl moieties of PFS in dichloromethane solution, whereas the reaction with I_2 does not proceed to completion.[47] These processes, however, are all complicated by the involvement of non-innocent counterions, which result in significant chain scission being detected after reduction back to the neutral state. We have previously found, however, that employing $[SbF_6]^-$ as the counterion to the oxidant facilitates oxidation/reduction cycles of PFS gels without detectable degradation.[48] This is presumably due to the less favorable thermodynamics of fluoride ion oxidation by the aminium cation, relative to that of the chloride ion, which has been invoked as the origin of the reactivity of $[SbCl_6]^-$.[49] Although chain scission was not apparent in the oxidation of the solvent-swollen PFS cores of cylindrical micelles with Ag(I), the formation of metallic Ag that was desirable in that instance would complicate the current study.[39b] We, therefore, chose to employ $[(4\text{-}BrC_6H_4)_3N][SbF_6]$ (Scheme 1) as the oxidant in this investigation, which had the added advantage of enabling the experiments to be followed by UV−vis spectroscopy, due to the colorless amine by product. The oxidation experiments were all conducted under a dry and inert atmosphere in dry dichloromethane to prevent decomposition of the oxidant,[50] and to enable the effective solvation of both polymer and oxidant.[51]

2. Redox-Induced Self-Assembly of PS_{548}-*b*-$PFMPS_{73}$ (4a) with $[N(C_6H_4\text{-}Br\text{-}4)_3][SbF_6]$ (1). A solution of **1** in dichloromethane (containing x equivalents with respect to the number of ferrocene moieties per chain) was added to a similar solution of **4a** over ca. 1 s. As the amount of oxidant added was increased, the color of the solution changed from orange, characteristic of the neutral block copolymer, through green and finally to intense blue for the fully oxidized samples. Figure 1A shows the typical UV−vis spectra of the neutral (x = 0.00) diblock copolymer, its partially oxidized derivatives (x = 0.05, 0.10, 0.25, 0.50 and 0.75) and the fully oxidized state (x = 1.00). As x increases, the absorbance that arises from the $d-d$ transition common to ferrocene at 450 nm decreases with a concomitant increase in that due to the ligand-to-metal charge transfer (LMCT) transition of ferricinium units at 640 nm. Furthermore, these decrease and increase, respectively, in direct relationship to the degree of oxidation (Figure 1B for the latter). The formation of some precipitate was observed at levels of oxidation of x > 0.5; however, the linear relationship obtained between x and the absorbance of the MLCT transition suggests that this represents a small portion of the material present. The oxidation of the ferrocene centers of the PFMPS block by **1** therefore provided a controlled method for oxidizing the diblock copolymer **4a**.

The morphologies of the species formed by **4a** at the various degrees of oxidation (x = 0.00, 0.05, 0.10, 0.25, 0.50, 0.75 and 1.00) were studied, in the first instance, by drop-casting samples onto carbon coated copper grids and imaging by TEM. For

dx.doi.org/10.1021/ja1105656 |*J. Am. Chem. Soc.* 2011, 133, 8903–8913

Scheme 1. (A) Hexafluoro− and Hexachloro−Antimonate Salts of the Tris(4-bromophenyl)-ammoniumyl Cation (1 and 2, respectively) and Decamethylcobaltocene (3). (B) Oxidation of PS-*b*-PFS Diblock Copolymers (4, 5, and 6) in Dichloromethane with either 1 or 2, and where $1 \geq x \geq 0$

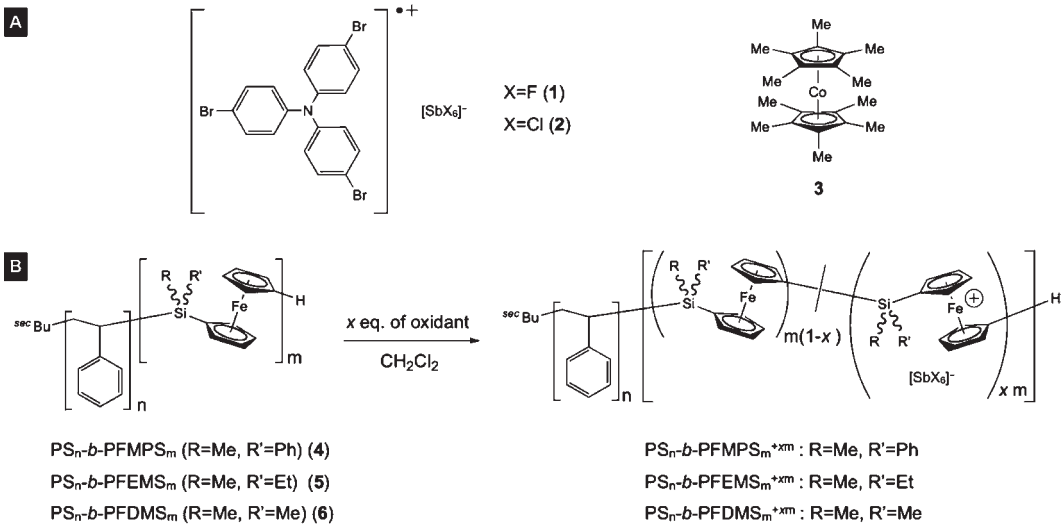

Table 1. Compositional Data for the PS-*b*-PFS Diblock Copolymers Studied

	block copolymers	$M_n \times 10^{-3}$ (g/mol)	Φ_{PFS}	PS to PFS ratio	PDI
4a	PS_{548}-*b*-$PFMPS_{73}$	79.3	0.24	7.5:1	1.08
4b	PS_{71}-*b*-$PFMPS_{165}$	57.6	0.84	1:2.3	1.17
5a	PS_{389}-*b*-$PFEMS_{108}$	69.1	0.36	3.6:1	1.04
5b	PS_{264}-*b*-$PFEMS_{881}$	253.2	0.87	1:3.3	1.17
6	PS_{535}-*b*-$PFDMS_{103}$	80.7	0.26	5.2:1	1.03

x = 0.00 and 0.05 (Figure 2A,B), a thin film of PFMPS cylinders within a matrix of PS was observed lying parallel to the substrate. This morphology is in keeping with that expected on the grounds of volume fraction (Φ_{PFS} = 0.24),[44] although the domain boundaries are poorly defined and there was little long-range order in the absence of an annealing step. For x = 0.10 and 0.25 (Figure 2C,D), the phase separation between the two domains became more distinct, presumably due to an increase in the Flory−Huggins interaction parameter, χ, on increasing the charge on the PFMPS block. Nonetheless, the samples still formed uniform films and no discrete micelles or micellar aggregates were observed. For x = 0.50, however, a discontinuity occurred in the morphological evolution. Although some areas of the sample showed a thin-film morphology that was more distinctly segregated than those previously discussed, well-defined spherical objects with electron-rich cores of 37 nm in diameter were also observed. These micelles became the exclusive morphology for degrees of oxidation of $x \geq 0.75$, with the diameters of the spheres decreasing with increasing x (28 nm for x = 0.75 and 23 nm for x = 1.00, Figure 2, panels G and H, respectively). The decrease in micelle size might be explained by either an increase in the density of the core, since the polymer has a higher degree of oxidation and becomes increasingly more incompatible with the solvent, or by the addition of fewer macromolecules per micelle due to the repulsion of the charged PFMPS chains. For x = 1.00, the spherical micelles were observed to aggregate in necklace-fashion, creating larger networks that may account for the small amount of precipitation observed (vide supra). This phenomenon could be explained by colloidal electrostatic self-assembly, similar to that observed by Cosgrove et al.,[53] or simply be the result of solvent evaporation during sample preparation.

The decrease in the hydrophobicity of the oxidized PFMPS chains, due to the increase in the charge upon oxidation, gave rise to micelle formation with the neutral organic block constituting the fully solvated corona and the partially oxidized organometallic segment forming the core. The formation of an insoluble core, and thus micellization, was possible only when a certain threshold degree in oxidation was reached. Before this point, bulk phase-separation was observed with the domain barriers becoming more distinct as the polarity difference between the PS and PFMPS blocks increased. This effect can be explained by the increasing immiscibility between the organic and the organometallic segments due on increasing the charge on the latter. Scheme 2 shows a schematic representation of the proposed morphologies obtained upon controlled oxidation of **4a** with **1**.

The oxidation induced micellization of **4a** was also studied in solution by DLS. Both unimeric and micellar entities were present at x = 0.50 (Figure 3A) with apparent hydrodynamic radii ($R_{h,\ app}$) of 3 and 70 nm, respectively. These findings were consistent with the coexistence of thin film and micellar morphologies observed by TEM. For x = 0.75, a single size distribution was observed with an $R_{h,\ app}$ = 34 nm (Figure 3B), and this supports the proposed transition to a solely micellar morphology on increasing the degree of oxidation, which was suggested by TEM data. When fully oxidized (x = 1.00, Figure 3C), the micelles were even smaller ($R_{h,\ app}$ = 27 nm) and this is again consistent with the trend of decreasing micellar size observed by TEM. It is noteworthy that the necklace-type aggregation of the spheres that was apparent in the TEM micrograph cannot be detected in solution, and this supports the assertion that drying effects may play a key role. A small quantity of precipitate, however, was also observed and it is possible that this may be the

dx.doi.org/10.1021/ja1105656 |J. Am. Chem. Soc. 2011, 133, 8903–8913

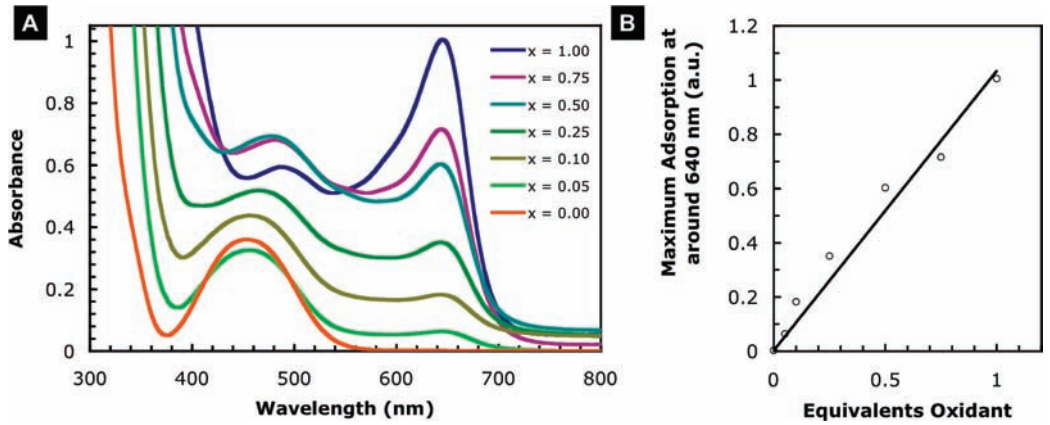

Figure 1. (A) UV−vis spectra of **4a** in dichloromethane for various molar ratios (x) of $[N(C_6H_4Br\text{-}4)_3][SbF_6]$ (**1**) added, and (B) the linear dependence of the absorbance of the ferricinium LMCT band with the molar ratio of the oxidant added. It should be noted that at no point is **1** ($\lambda_{max} \approx 700$ nm)[52] detected.

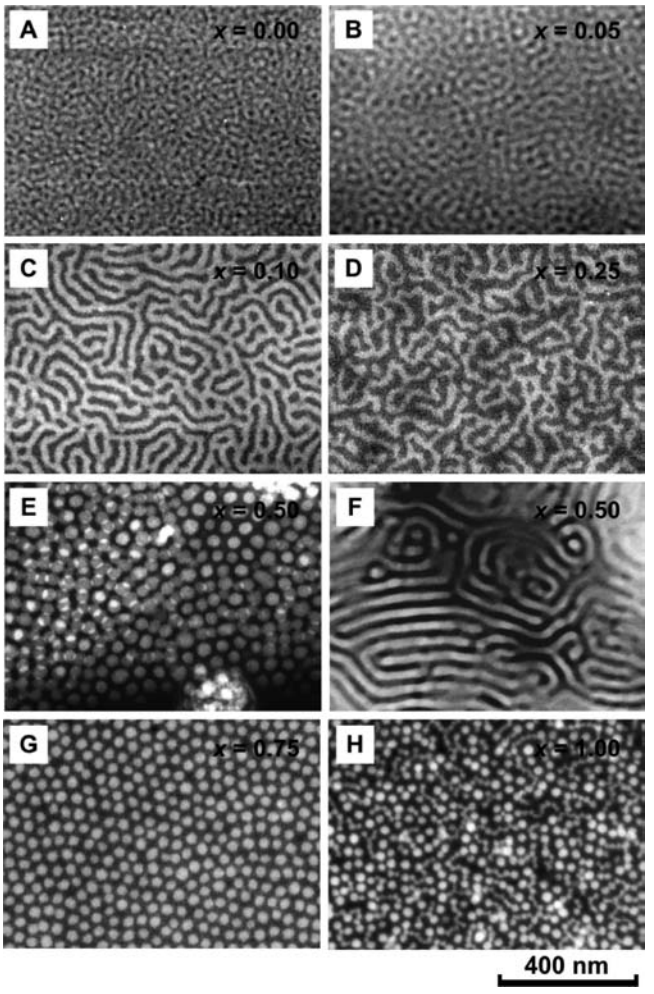

Figure 2. Dark field TEM images of the redox response of **4a** to the addition of increasing amounts of **1**. (A) Image represents the neutral block copolymer (x = 0.00); (B−H) the images for x = 0.05, 0.10, 0.25, 0.50 (E and F), 0.75 and 1.00, respectively.

result of such a process. We postulate that it is this reduction in the concentration of micelles in colloidal solution, relative to that of unimer, that enables the latter to be observed by DLS in this

Scheme 2. Schematic Representation of the Controlled Oxidation of 4a with x equiv of 1

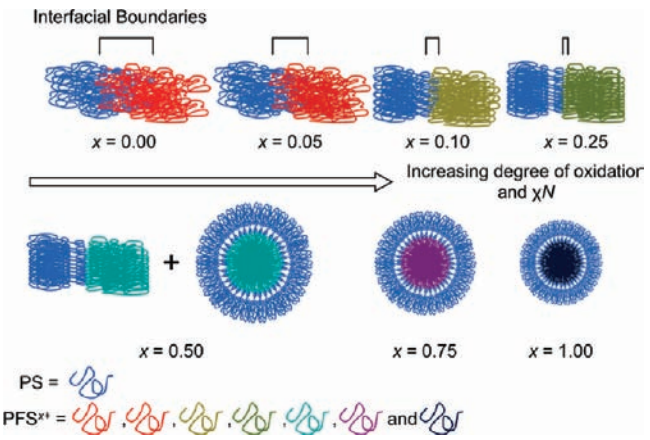

instance, albeit as a very low intensity peak (Figure 3C), whereas the presumably more soluble chains could not be observed when x = 0.75 (Figure 3B).

3. Reduction and Disassembly of Spherical Micelles of PS_{548}-*b*-$PFMPS_{73}$ (4a) Using $[N(C_6H_4\text{-}Br\text{-}4)_3][SbF_6]$ (1) as Oxidant and $[Co(\eta\text{-}C_5Me_5)_2]$ (3) as Reductant. The reversibility of the oxidation and hence the disassembly of the micelles was studied by treatment of the oxidized samples with the strong reductant $[Co(\eta\text{-}C_5Me_5)_2]$ (**3**) ($E^{0'} = -1.94$ V vs ferrocene)[54] in dichloromethane. The change in color from blue-green to orange was an indication of the reduction of the ferricinium centers to neutral ferrocene moieties. This was confirmed by the UV−vis spectrum after the addition of 1 equiv of **3** per ferrocene unit to a sample of **4a** that had previously been completely oxidized by **1**. In this case, no MLCT transition, characteristic of ferricinium moieties, was observed (Figure 4A).

Upon reduction, there were no signs of significant chain cleavage, as indicated by the GPC data for **4a** after being oxidized with **1** and then reduced with **3**. The GPC traces from before and after oxidation/reduction are similar, both showing a low PDI and the same molecular weight, within experimental error (Figure 4B). The reduced diblock copolymer was completely recovered, affording unimers in dichloromethane, and no micellar

dx.doi.org/10.1021/ja1105656 |*J. Am. Chem. Soc.* 2011, 133, 8903–8913

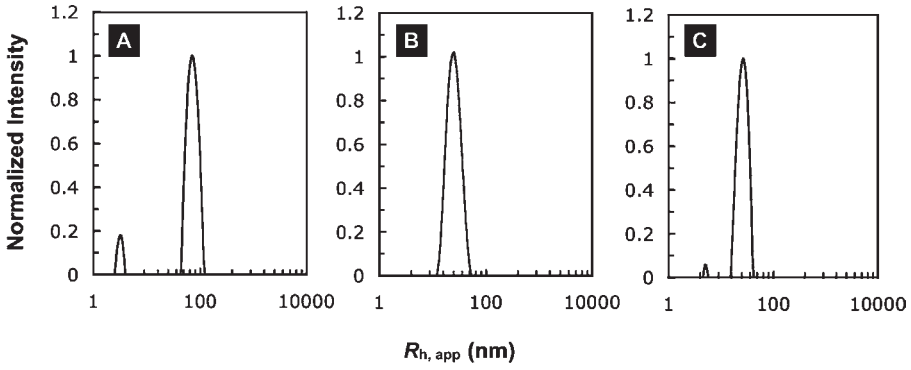

Figure 3. Dynamic light scattering (DLS) CONTIN plots at room temperature, in dichloromethane, for **4a** after addition of (A) $x = 0.50$, (B) $x = 0.75$, and (C) $x = 1.00$ equiv of **1** per ferrocene unit.

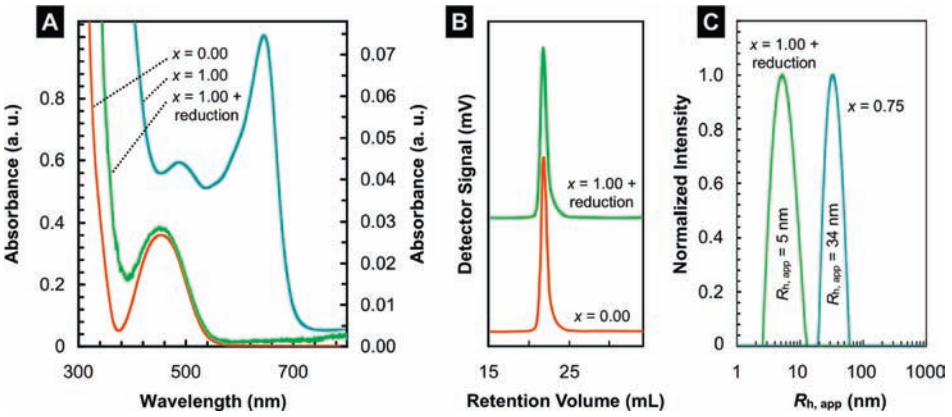

Figure 4. (A) UV−vis spectra of the neutral ($x = 0.00$), oxidized ($x = 1.00$) and reduced form of **4a** in dichloromethane. The reduction was performed on **4a** with **3** after complete oxidation with **1**. (B) GPC traces in THF of **4a** as synthesized ($x = 0.00$) and reduced following complete oxidation with **1**. (C) DLS plots of the micellar aggregates from **4a** when oxidized ($x = 0.75$) with **1**, and the unimeric, neutral **4a** after reduction with **3**.

aggregates were found in solution using DLS techniques (Figure 4C). These results demonstrate that micellar disassembly was due to complete reduction of intact diblock copolymer chains and not macromolecular chain scission.

4. Redox-Induced Self-Assembly of PS_{548}-*b*-$PFMPS_{73}$ (4a) Using $[N(C_6H_4\text{-Br-}4)_3][SbCl_6]$ (2). To examine the effect of the counterion on the micellar size, we studied the oxidation of **4a** with tris(4-bromophenyl)-ammoniumyl hexachloroantimonate ($[N(C_6H_4Br\text{-}4)_3][SbCl_6]$, **2**), also in dichloromethane solution.

The controlled oxidation of the ferrocene units of the polymer **4a** with **2** in dichloromethane was followed by UV−vis spectroscopy (Figure S1). As was the case in the oxidation of **4a** with **1**, the intensity of the absorbance arising from the ferricinium site scaled linearly with the amount of oxidant added.

The self-assembly behavior of **4a** when oxidized with **2** was broadly similar to that observed with **1**. Thus, imaging by TEM indicated a transition from thin-film to micellar morphologies at $x \geq 0.5$ and the latter were spherical in nature (Figure 5). Interestingly, these micelles were on average larger than those formed on oxidation by **1**. In Figure 5A, which corresponds to $x = 0.50$, spherical micelles are evident, but these are visibly more polydisperse in nature than those obtained with **1**. Their sizes ranged from 20 to 110 nm (with an average diameter of 55 nm and a σ of 13.6 nm). A more uniform size distribution was obtained with $x = 0.75$, with the standard deviation ($\sigma = 9.5$ nm) representing a smaller fraction of the average diameter (69 nm, Figure 5B). Similar to the situation observed in the case of the smaller $[SbF_6]^-$ counterion, a necklace-type aggregation of the spherical micelles (diameter = 64 nm, $\sigma = 8.6$ nm) occurred when the organometallic block was fully oxidised ($x = 1.00$, Figure 5C). The DLS study supported the observations made by TEM and revealed an increase in the hydrodynamic radius as x increased and more counterions were added to the core ($R_{h,\,app}$ = 61 and 84 nm for $x = 0.50$ and 0.75, see Figure S2). For $x = 1.00$, only very large aggregates were observed by DLS, which suggested that formation of the necklace-type aggregates may be detectable in solution. Although the change of anion did not alter the oxidation threshold for micelle formation or the morphologies observed, this series did not follow the trend in which the micelle size decreased with increasing x. The addition of the $[SbCl_6]^-$ counterion, which is ca. twice as large as the $[SbF_6]^-$ anion,[55] might be expected to overcome the core shrinkage observed with increasing x in the series oxidized with **1**. Nevertheless, as the core sizes of the micelles formed upon oxidation varied with the counterion used, we could conclude that the counterion was present mainly in the dense core of the micelles. Figure 6A shows a TEM image of **4a** oxidized at $x = 0.75$ with **2**. An energy dispersive X-ray (EDX) line analysis was traced along 6 spherical micelles (Figure 6). Alternating counts for the different elements are observed, being correlated to the high and low electron contrast on

dx.doi.org/10.1021/ja1105656 |*J. Am. Chem. Soc.* 2011, 133, 8903–8913

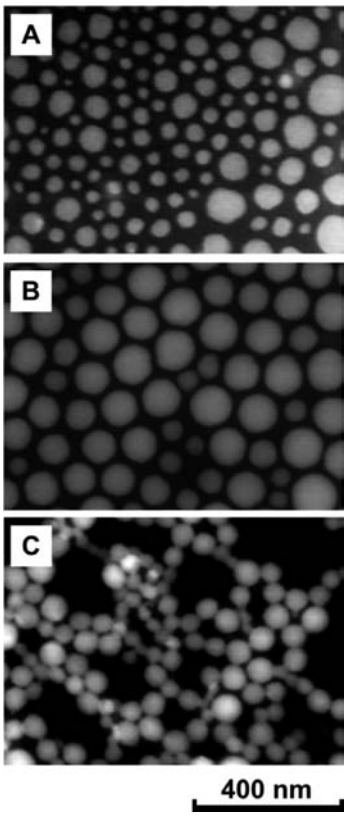

Figure 5. Dark field TEM images of the response of **4a** to the addition of increasing amounts of **2**. (A–C) represent x = 0.50, 0.75 and 1.00, respectively.

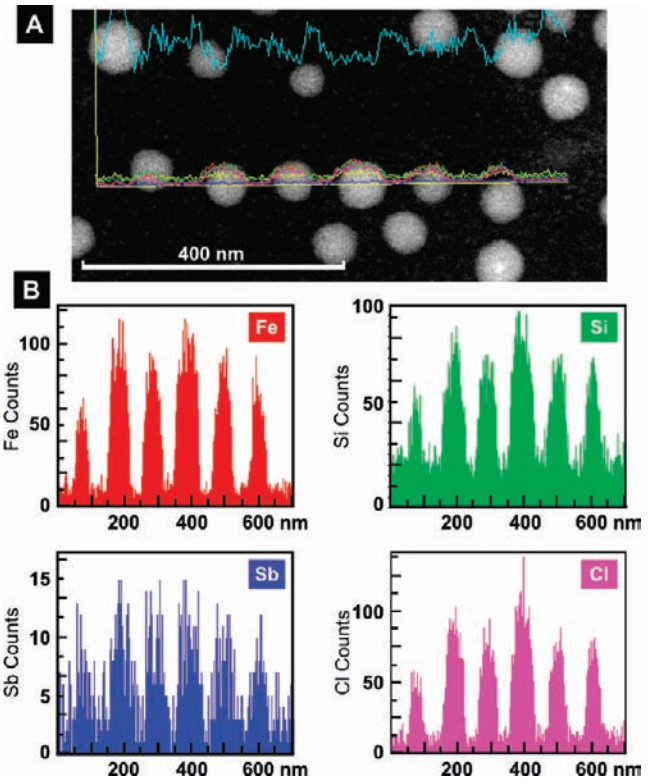

Figure 6. (A) Dark field TEM image of **4a** oxidized by **2** at x = 0.75 in dichloromethane. (B) Energy dispersive X-ray analysis for iron, silicon, antimony and chlorine along the line traced across 6 spherical micelles.

the TEM image. The presence of iron, silicon, antimony and chlorine was confirmed only in the core of the micelle and the ratio of counts between iron and silicon was 1:1 and between antimony and chlorine was ca. 1:6. This data is consistent with the anticipated core structure of oxidized PFMPS with $[SbCl_6]^-$ counterions.

We also conducted a ^{1}H NMR spectroscopic study on the micelle solutions that had been produced directly in CD_2Cl_2. The deuterated solution contained both the oxidized micelles and the soluble aromatic amine byproduct from the reduction of the oxidant. The integration ratio of the byproduct amine $[N(C_6H_4Br\text{-}4)_3]$ peak (CD_2Cl_2, δ 7.37) versus a PS peak (CD_2Cl_2, δ 6.59) was plotted against x (see Figure S3). Beside the evidence for good solvation of the coronal PS block, the NMR study revealed that the amount of amine increased linearly with x, indicating that it was present mainly outside the insoluble core.

The reversibility of the oxidation was tested by reduction with **3** of oxidized **4a** bearing $[SbCl_6]^-$ counterions (Figure S4). Despite UV–vis spectroscopy indicating complete reduction of all the ferricinium centers, a bimodal distribution for the GPC trace and a smaller $R_{h,\,app}$ based on DLS were observed, which indicated the presence of polymers with lower molecular weights. This implied that chain cleavage may occur prior to redox-induced micellization when **2** is employed as the oxidant.[49] The larger micelle size dispersity that was observed (Figure 5), when compared to analogous structures prepared with **1** (Figure 2), may result from the presence of block copolymers with a distribution of PFS segment lengths.

5. Redox-Induced Self-Assembly of PS_{71}-b-$PFMPS_{165}$ (4b) with $[N(C_6H_4\text{-}Br\text{-}4)_3][SbF_6]$ (1). To examine the effect of decreasing the length of the corona-forming PS block, the redox-induced self-assembly of another block copolymer, **4b** (Table 1), was investigated. This material contained a significantly higher PFMPS volume fraction (Φ_{PFMPS} = 0.84) than **4a** (Φ_{PFMPS} = 0.24), and thus would be expected to form crew-cut micelles rather than spheres.[2,3]

The oxidation of **4b** with **1** was controlled, as evidenced by a linear relationship between the intensity of the MLCT absorbance arising from the ferricinium units and x (Figure S5). Analysis of the solutions by TEM demonstrated thin-film morphologies for x < 0.50, in which the domain boundaries became more distinct with increasing degrees of oxidation (see Figure S7). As with **4a**, the formation of micelles was triggered by the oxidation of half of the ferrocene moieties in the organometallic block (Figure 7A, x = 0.50) and these were again spherical. The resulting spheres possessed an average estimated diameter of 40 nm. When further oxidized (x = 0.75, Figure 7B), the micelles remained spherical and had a smaller average diameter of 21 nm. When fully oxidized (x = 1.00, Figure 7C), the observed spherical micelles were smaller than both those for x = 0.50 and 0.75, with an average diameter of 17 nm. Contrary to the similar situation observed for **4a**, no necklace-type aggregation was observed in this instance.

Although the PFS block in **4b** was twice as long as in **4a**, the cores from the crew-cut micelles had slightly smaller sizes according to the TEM images. It is possible that an enthalpic contribution may exist that prevented the formation of larger cores, reducing the number of diblock copolymer chains per micelle. Table 2 summarizes the micelle sizes obtained in different oxidation series. As with the case of the oxidation of **4a** with **1**, reduction with **3** regenerated the original unimers

dx.doi.org/10.1021/ja1105656 |*J. Am. Chem. Soc.* 2011, 133, 8903–8913

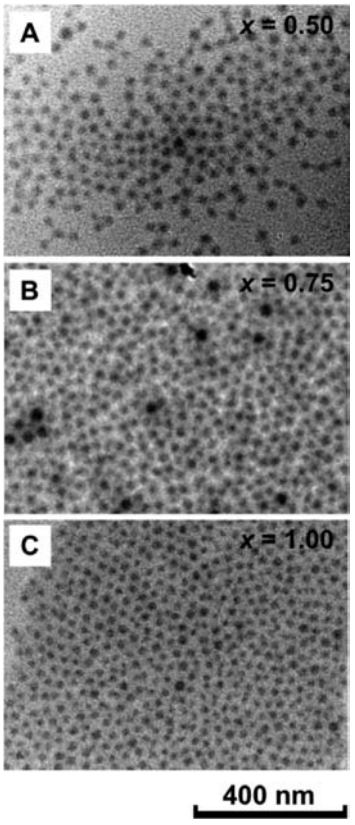

Figure 7. Bright field TEM images of the redox response of **4b** upon addition of increasing amounts of **1** in dichloromethane. (A−C) Images for x = 0.50, 0.75 and 1.00, respectively.

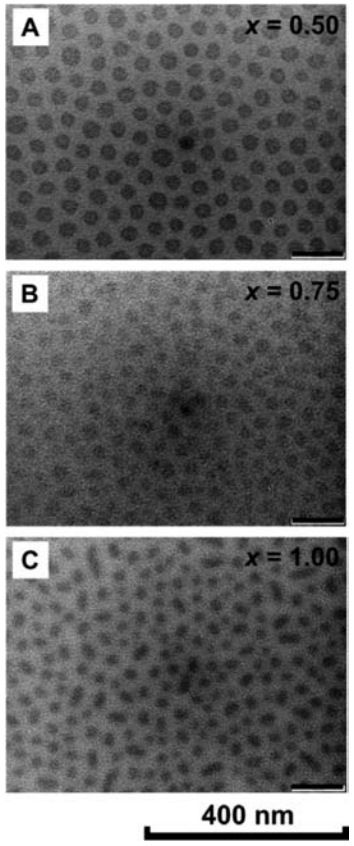

Figure 8. Bright field TEM images of the redox response of **5a** upon addition of increasing amounts of **1** in dichloromethane. (A−C) Images for x = 0.50, 0.75 and 1.00, respectively.

Table 2. Core Diameters and Hydrodynamic Radii of the Spherical Micelles Obtained by Redox-Induced Self-Assembly

diblock copolymer	oxidant	x	core diameter, nm (SD)[a]	$R_{h,\ app}$, nm[b]
4a	**1**	0.50	37 (4.7)	70
Φ_{PFMPS} = 0.24		0.75	28 (3.0)	34
		1.00	23 (3.0)	27
4a	**2**	0.50	55 (13.6)	61
Φ_{PFMPS} = 0.24		0.75	69 (9.5)	84
		1.00	64 (8.6)	>200
4b	**1**	0.50	40 (5.4)	21
Φ_{PFMPS} = 0.84		0.75	21 (1.7)	24
		1.00	17 (3.4)	26
5a	**1**	0.50	25 (2.8)	30
Φ_{PFEMS} = 0.36		0.75	25 (1.9)	22
		1.00	19 (2.0)	23
5b	**1**	0.50	83 (17.0)	30
Φ_{PFEMS} = 0.87		0.75	51 (8.9)	24
		1.00	35 (3.7)	27

[a] Diameter determined by measuring the diagonal of the electron-dense areas on TEM images for 40 objects. [b] Apparent hydrodynamic radius obtained by DLS in dichloromethane at 25 °C.

quantitatively thereby demonstrating the reversibility of the micellization process.

6. Redox-Induced Self-Assembly of PS_{389}-*b*-$PFEMS_{108}$ (5a) and PS_{264}-*b*-$PFEMS_{881}$ (5b) with $[N(C_6H_4\text{-Br-}4)_3][SbF_6]$ (1).

To provide further insight into the redox-controlled micellization of PS-*b*-PFS diblock copolymers, we studied the effect of changing the relatively rigid amorphous PFMPS block ($T_g \sim 90$ °C)[27] for the more flexible amorphous PFEMS segment ($T_g \sim 25$ °C)[44] with ethyl and methyl substituents at silicon.

Two materials, **5a** and **5b**, with Φ_{PFEMS} = 0.36 and 0.87, respectively, (Table 1) were examined under the same conditions as those used for the treatment of **4a** and **4b** with **1**. The consumption of the oxidant was stoichiometric and the absorbance of the LMCT band proved to be linear with respect to the number of equivalents of **1** added in both cases (see Figures S8 and S10 for the UV−vis spectra). Analysis by TEM revealed the formation of spherical micelles starting from x = 0.50 through x = 1.00 for both **5a** and **5b** (Figures 8 and 9, respectively). The dimensions observed by TEM revealed a decrease in the core diameter as the degree of oxidation increased (for **5a**, 25, 25, and 19 nm for x = 0.50, 0.75 and 1.00, respectively and for **5b**, 83, 51, and 35 nm for x = 0.50, 0.75 and 1.00, respectively). A significant micelle fusion effect was detected for **5b** (see Figure 9A−C). In this case, the PFS block was larger (8 times longer than that present in **5a**) and the material had a higher polydispersity (PDI = 1.17). This effect is likely to be promoted by a low T_g core, due to improved chain mobility. The observation of similar aggregation with the PFMPS-containing micelles and the independence of this process on coronal chain length, however, suggests that drying effects and core plasticization, for example, may also be operative. Reduction of the oxidized block copolymer micelles derived from **5a** and **5b** with **3** afforded the full recovery of the original unimers in each case.

dx.doi.org/10.1021/ja1105656 |*J. Am. Chem. Soc.* 2011, 133, 8903–8913

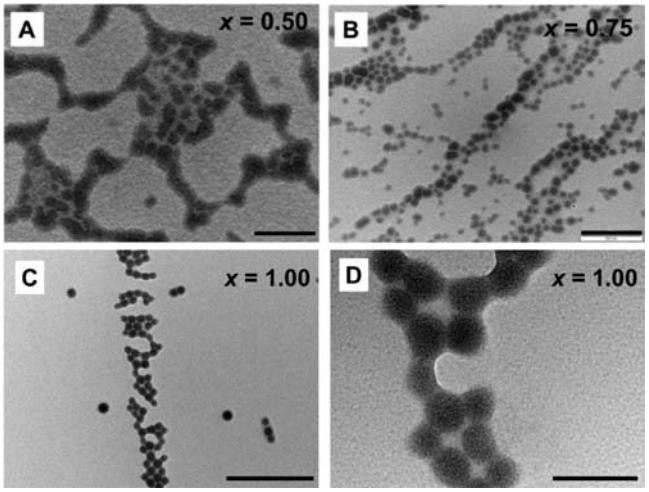

Figure 9. Bright field TEM images of the redox response of **5b** upon addition of increasing amounts of **1** in dichloromethane. (A–C) Images for $x = 0.50$, 0.75 and 1.00, respectively; (D) high magnification image of the micelles for $x = 1.00$. Scale bars are for 500 nm except for (D), 100 nm.

7. Redox-Induced Self-Assembly of PS_{535}-*b*-$PFDMS_{103}$ (6) with $[N(C_6H_4\text{-Br-}4)_3][SbF_6]$ (1). The spherical PS-*b*-PFS block copolymer micelles studied so far in the current work possessed amorphous PFS core-forming blocks. Previous studies have shown that block copolymers with a semicrystalline PFS core-forming block prefer to form morphologies with low interfacial curvature when self-assembled in solution.[56−61] We therefore also explored the redox-induced micellization of PS_{535}-*b*-$PFDMS_{103}$ (**6**) with the view to preparing micelles with nonspherical structures.

The controlled oxidation procedure described earlier was applied to **6** using **1** as the oxidant in dichloromethane solutions. In a similar manner to the block copolymers with an amorphous PFS block, PS-*b*-PFDMS (**6**) ($\Phi_{PFDMS} = 0.26$), with a semicrystalline PFS segment, was oxidized controllably from $x = 0.00$ to 1.00 in CH_2Cl_2 as confirmed by the linear increase in the absorbance of the LMCT band from UV–vis spectroscopy (see Figure S13). DLS studies suggested that unimers were present in solution with degrees of oxidation up to $x = 0.25$ ($R_{h,\ app} \approx 5$ nm). For $x = 0.25$, however, the amount of unimers was found to significantly decrease ca. 2.5 h after the addition of **1**, affording a new size population ($R_{h,\ app} = 199$ nm) and a small quantity of blue-green precipitate. No unimers could be detected by DLS after 45 h and the size of the colloidal particles remained in the range of ca. 165–255 nm until the experiment was concluded after 117 h. Analysis of the colloidal solution by TEM at any point after the initial 2.5 h period indicated the formation of large aggregates composed of smaller platelets (Figure S14C).

For $x = 0.5$, the self-assembly process was well-established only 3 h after the addition of **1** with no remaining unimers and only a single new size population ($R_{h,\ app} = 30$ nm) detectable by DLS. The size distribution then remained effectively unchanged until 45 h at which point the dominant population was significantly larger in size ($R_{h,\ app} = 430$ nm), and the formation of a blue-green precipitate was observed. Over the following 120 h, no significant change was observed by DLS with the size of the population increasing gradually to a maximum value of 450 nm. Analysis of the solutions by TEM after solvent evaporation revealed the presence of wavy ribbon-like micelles (narrow platelets)

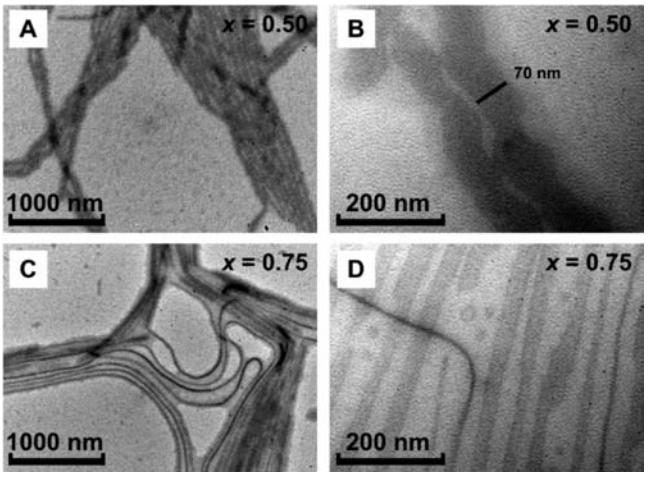

Figure 10. Bright field TEM images of **6** oxidized with **1** in dichloromethane. (A and B) $x = 0.50$; (C and D) $x = 0.75$, after 120 hours.

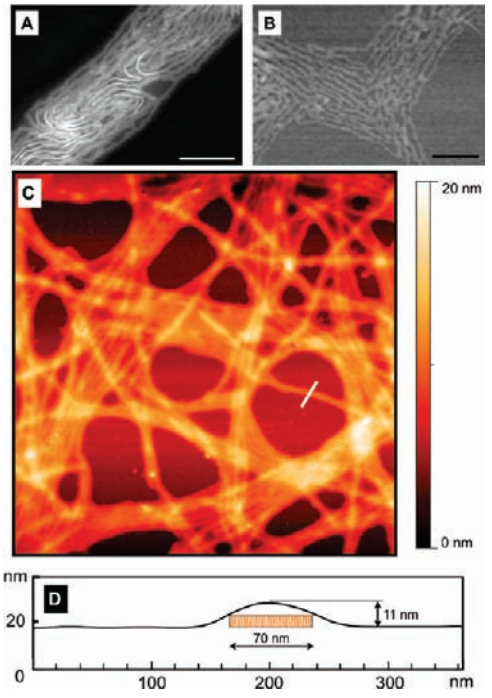

Figure 11. (A) Dark field TEM image of **6** oxidized with **1** for $x = 0.50$, scale bar 300 nm, (B) SEM image of the bare core obtained by removal of the PS corona under an Ar plasma for 10 mins, scale bar 300 nm, (C) AFM height image of bundles of micelles, and (D) height profile (expanded in the *z*-direction) of the AFM image (white trace) with a cartoon representing the space taken by the core of one micelle.

of several micrometers in length and about 70 nm in width (Figure 10A,B). It was also possible to detect the PS corona as a gray halo around the denser iron-rich PFS core in Figure 10B. A ribbon rather than a cylindrical morphology was assigned, as it was possible to image the structures orientated perpendicular to the substrate, thus, casting a denser shadow on the TEM (see Figure 11A for an example). The SEM image (Figure 11B) showing the bare core of the micelles was obtained after removing the organic PS corona under an argon plasma,[62] and confirmed the irregularity of the ribbons. AFM analysis (Figure 11C,D) was not able to discern

the core but showed a height of 11 nm and a width of 70 nm, which corresponded well to the core width measured under bright field TEM (Figure 10B).

Interestingly, experiments at a higher oxidation level ($x = 0.75$) revealed only unimers by DLS until 5.5 h after the addition of **1** to **6**. These evolved, however, into large aggregates ($R_{h,\ app}$ = 520 nm) after 24 h, which increased further in size at 46.5 h ($R_{h,\ app}$ = 840 nm). As previously observed at lower levels of oxidation, aggregation was also accompanied by the precipitation of a blue-green solid. Analysis of the solution by TEM at various stages of micelle maturation indicated the coexistence of small spherical micelles (15 nm diameter) and long ribbons (see Figure 10C,D). It is likely that the large aggregates dominate the scattering detected using DLS and that this prevented the smaller spheres from being observed. The competition between oxidation-induced self-assembly and crystallization of the PFDMS block appeared to make this particular system difficult to study. For example, significant variations in the relative amounts of the different morphologies were detected as a function of time in apparently identical experiments. Indeed, in some cases, only spherical micelles of 15 nm in radius were observed by TEM in conjunction with the observation of a single size population by DLS ($R_{h,\ app}$ = 25 nm). Nevertheless, these results and the WAXS data (see below) for the x = 0.75 system are reminiscent of the slow transformation of amorphous spheres to crystalline cylinders previously detected for PFDMS-*b*-P2VP (P2VP = poly(2-vinylpyridine) in EtOH, a selective solvent for the P2VP block.[63] In addition, it is noteworthy that complete oxidation of **6** by **1** (x = 1.0) afforded only polydisperse spherical micelles between 50 and 150 nm in diameter, although studying the evolution of these species by DLS proved problematic, presumably due to precipitation of the material.

To evaluate the proposition that the nonspherical shape of the micelles was the result of core crystallization, as has been previously demonstrated for neutral PFDMS-containing systems,[56−61] the ribbons obtained from **6** at $x = 0.50$ were studied by wide-angle X-ray scattering (WAXS). The resulting diffraction pattern (Figure S15) exhibited sharp peaks at 2θ values of 12.9, 16.7, 22.0, 23.7, 25.8 and 39.2°, in addition to a broad amorphous halo centered at $2\theta \approx 19.2°$. The sharp features are consistent with the presence of crystalline domains within the micellar cores, and the most intense reflection ($2\theta = 12.9°$) corresponds to a lattice-spacing, d, of 6.86 Å. If this parameter is interpreted as the interchain separation, as has been proposed for solution crystallized PFDMS and self-assembled $PFDMS_{50}$-*b*-$PDMS_{300}$ (d = 6.34 and 6.3 Å, respectively),[57,61a] then **6** crystallizes in an expanded lattice after oxidation. Such a change is consistent with the requirement for counterion incorporation into the lattice, so as to maintain a charge-neutral structure. These data should be contrasted with the WAXS diffraction pattern that was obtained from spherical micelles formed from **4a** when oxidized with **1** to $x = 0.75$ (Figure S15), which exhibited only an amorphous halo ($2\theta \approx 19.6°$). Furthermore, the spherical micelles observed for **6** at x = 0.75 also afforded an effectively featureless diffraction pattern (Figure S15). This result is consistent with the postulate that the spherical objects present in the mixture are indeed amorphous.

Subsequent reduction of **6** (x = 0.50) with **3** afforded the recovery of the neutral unimers as attested by UV−vis, where no LMCT band was observed in the 600−700 wavelength nm region, DLS, where the $R_{h,\ app}$ value returned to that prior to oxidation, and GPC, which showed a monomodal trace overlaying that of the neutral diblock prior to oxidation (see Figures S16A, B and C). This confirmed that the redox-induced micellization of **6** oxidized with **1** to form ribbon like micelles is also fully reversible, as for the cases of the amorphous analogues **4a**, **4b**, **5a**, and **5b**.

SUMMARY

We report a detailed study of the resulting micelle morphologies formed by PS-*b*-PFS diblock copolymers when these materials were oxidized to varied extents ($0 < x \leq 1$) in solution with hexahaloantimonate salts of the tris(4-bromophenyl)-ammoniumyl cation. Amorphous PS-*b*-PFS materials gave well-defined spherical micelles after oxidation with a fully solvated PS corona and an oxidized PFS core in dichloromethane. The $[SbX_6]^-$ counterions were located within the core. Effective micelle disassembly was observed on reduction with decamethylcobaltocene, releasing free unimeric chains of the neutral diblock copolymer. The process showed excellent reversibility with the $[SbF_6]^-$ counterion, but a significant degree of irreversibility where the non-innocent $[SbCl_6]^-$ counterion was employed. An alteration of the substituents on the silicon, as well as the variation of the block ratio of the amorphous copolymers, did not affect the preferred spherical morphology for the micelles. In contrast, the use of a crystalline PFS block played an important role in changing the morphology from spheres to ribbons. This indicated that the presence of a crystalline oxidized PFS core plays a similar role in promoting the formation of micelles with low interfacial curvature as previously found for neutral PFS materials.[56−61] All amorphous micelles were created spontaneously from a threshold of x = 0.50, corresponding to the oxidation of half of the ferrocene moieties per polymer chain. The micellar dimensions were dictated by the competition between charge counts, added volume of counterions, and polarity change (solvophobicity). The work demonstrated that a redox stimulus is a versatile tool with which to control the self-assembly of block copolymers, which may prove useful in applications where other stimuli-responsive materials are currently employed.

ASSOCIATED CONTENT

Supporting Information. Materials, experimental procedures; selected DLS, UV−visible spectroscopic and WAXS data; selected TEM and AFM images. This material is available free of charge via the Internet at http://pubs.acs.org.

AUTHOR INFORMATION

Corresponding Author

ian.manners@bristol.ac.uk; mwinnik@chem.utoronto.ca

Present Address

[§]Departments of Chemistry and Engineering Technology, Western Washington University, Bellingham, Washington 98225, United States.

ACKNOWLEDGMENT

I.M. wishes to thank the EU, EPSRC, and the University of Bristol for funding this research. M.A.W also thanks NSERC Canada for financial support.

REFERENCES

(1) For reviews on block copolymer self-assembly in solution see: (a) Discher, D. E.; Eisenberg, A. *Science* **2002**, *297*, 967–973. (b) Hamley, I. W. *Angew. Chem., Int. Ed.* **2003**, *42*, 1692–1712. (c) Lazzari, M.; López-Quintela, M. A. *Adv. Mater.* **2003**, *15*, 1583–1594. (d) Gohy, J.-F. *Adv. Polym. Sci.* **2005**, *190*, 65–136.

(2) Zhang, L.; Eisenberg, A. *Science* **1995**, *268*, 1728–1731.

(3) Zhang, L.; Yu, K.; Eisenberg, A. *Science* **1996**, *272*, 1777–1779.

(4) Pochan, D. J.; Chen, Z.; Cui, H.; Hales, K.; Qi, K.; Wooley, K. L. *Science* **2004**, *306*, 94–97.

(5) Li, Z.; Kesselman, E.; Talmon, Y.; Hillmyer, M. A.; Lodge, T. P. *Science* **2004**, *306*, 98–101.

(6) Geng, Y.; Dalhaimer, P.; Cai, S.; Tsai, R.; Tewari, M.; Minko, T.; Discher, D. E. *Nat. Nanotechnol.* **2007**, *2*, 249–255.

(7) Hu, J.; Liu, G.; Nijkang, G. *J. Am. Chem. Soc.* **2008**, *130*, 3236–3237.

(8) Dupont, J.; Liu, G.; Niihara, K.; Kimoto, R.; Jinnai, H. *Angew. Chem., Int. Ed.* **2009**, *48*, 6144–6147.

(9) Schacher, F.; Walther, A.; Ruppel, M.; Drechsler, M.; Müller, A. H. E. *Macromolecules* **2009**, *42*, 3540–3548.

(10) Rijcken, C. J. F.; Soga, O.; Hennink, W. E.; van Nostrum, C. F. *J. Controlled Release* **2007**, *120*, 131–148.

(11) Sundararaman, A.; Stephan, T.; Grubbs, R. B. *J. Am. Chem. Soc.* **2008**, *130*, 12264–12265.

(12) Moughton, A. O.; O'Reilly, R. K. *Chem. Commun.* **2010**, *46*, 1091–1093.

(13) Rodríguez-Hernández, J.; Lecommandoux, S. *J. Am. Chem. Soc.* **2005**, *127*, 2026–2027.

(14) Lee, H.; Lee, J. A.; Poon, Z.; Hammond, P. T. *Chem. Commun.* **2008**, 3726–3728.

(15) Lee, H.; Wu, W.; Oh, J. K.; Mueller, L.; Sherwood, G.; Peteanu, L.; Kowalewski, T.; Matyjaszewski, K. *Angew. Chem., Int. Ed.* **2007**, *46*, 2453–2457.

(16) For work on pH and temperature dependent micellization see: (a) Jiang, X.; Zhao, B. *Macromolecules* **2008**, *41*, 9366–9375. (b) Cai, C.; Zhang, L.; Li, J.; Wang, L. *J. Phys. Chem. B* **2008**, *112*, 12666–12673.

(17) For work on light and temperature dependent micellization see: Jiang, X.; Lavender, C. A.; Woodcock, J. W.; Zhao, B. *Macromolecules* **2008**, *41*, 2632–2643.

(18) For work on low molecular weight surfactants see: (a) Gallardo, B. S.; Gupta, V. K.; Eagerton, F. D.; Jong, L. I.; Craig, V. S.; Shah, R. R.; Abbott, N. L. *Science* **1999**, *283*, 57–60. (b) Aydogan, N.; Abbott, N. L. *Langmuir* **2001**, *17*, 5703–5706.

(19) Napoli, A.; Valentini, M.; Tirelli, N.; Müller, M.; Hubbell, J. A. *Nat. Mater.* **2004**, *3*, 183–189.

(20) Dahmane, S.; Lasia, A.; Zhao, Y. *Macromol. Chem. Phys.* **2008**, *209*, 1065–1072.

(21) Ma, N.; Li, Y.; Xu, H.; Wang, Z.; Zhang, X. *J. Am. Chem. Soc.* **2010**, *132*, 442–443.

(22) Bigot, J.; Charleux, B.; Cooke, G.; Delattre, F.; Fournier, D.; Lyskawa, J.; Sambe, L.; Stoffelbach, F.; Woisel, P. *J. Am. Chem. Soc.* **2010**, *132*, 10796–10801.

(23) Kim, H.; Jeong, S.-M.; Park, J.-W. *J. Am. Chem. Soc.* **2011**, *133*, 5206–5209.

(24) (a) Power-Billard, K. N.; Spontak, R. J.; Manners, I. *Angew. Chem., Int. Ed.* **2004**, *43*, 1260–1264. (b) Rider, D. A.; Winnik, M. A.; Manners, I. *Chem. Commun.* **2007**, 4483–4485. (c) Xiao, Z.-P.; Cai, Z.-H.; Liang, H.; Lu, J. *J. Mater. Chem.*, **2010**, *20*, 8375–8381. (d) Yan, Q.; Yuan, J.; Cai, Z.; Xin, Y.; Kang, Y.; Yin, Y. *J. Am. Chem. Soc.* **2010**, *132*, 9269–9270. (e) Zhu, L.; Shangguan, Y.; Sun, Y.; Ji, J.; Zheng, Q. *Soft Matter* **2010**, *6*, 5541–5546. (f) Xiao, Z.-P.; Cai, Z.-H.; Liang, H.; Lu, J. *J. Mater. Chem.* **2010**, *20*, 8375–8381.

(25) Yan, Y.; Lan, Y.; de Keizer, A.; Drechsler, M.; Van As, H.; Cohen Stuart, M. A.; Besseling, N. A. M. *Soft Matter* **2010**, *6*, 3244–3248.

(26) Plamper, F. A.; Murtomäki, L.; Walther, A.; Kontturi, K.; Tenhu, H. *Macromolecules* **2009**, *42*, 7254–7257.

(27) Manners, I. *Chem. Commun.* **1999**, 857–865.

(28) Manners, I. *Science* **2001**, *294*, 1664–1666.

(29) Bellas, V.; Rehahn, M. *Angew. Chem., Int. Ed.* **2007**, *46*, 5082–5104.

(30) Rulkens, R.; Lough, A. J.; Manners, I.; Lovelace, S. R.; Grant, C.; Geiger, W. E. *J. Am. Chem. Soc.* **1996**, *118*, 12683–12695.

(31) Pannell, K. H.; Dementiev, V. V.; Li, H.; Cervantes-Lee, F.; Nguyen, M. T.; Diaz, A. F. *Organometallics* **1994**, *13*, 3644–3650.

(32) Arsenault, A. C.; Puzzo, D. P.; Manners, I.; Ozin, G. A. *Nat. Photonics* **2007**, *1*, 468–472.

(33) Puzzo, D. P.; Arsenault, A. C.; Manners, I.; Ozin, G. A. *Angew. Chem., Int. Ed.* **2009**, *48*, 943–947.

(34) Hempenius, M. A.; Cirmi, C.; Song, J.; Vancso, G. J. *Macromolecules* **2009**, *42*, 2324–2326.

(35) Péter, M.; Hempenius, M. A.; Kooij, E. S.; Jenkins, T. A.; Roser, S. J.; Knoll, W.; Vancso, G. J. *Langmuir* **2004**, *20*, 891–897.

(36) Ma, Y.; Dong, W.-F.; Hempenius, M. A.; Möhwald, H.; Vancso, G. J. *Nat. Mater.* **2006**, *5*, 724–729.

(37) Shi, W.; Giannotti, M. I.; Zhang, X.; Hempenius, M. A.; Schönherr, H.; Vancso, G. J. *Angew. Chem., Int. Ed.* **2007**, *46*, 8400–8404.

(38) (a) Kulbaba, K.; Cheng, A.; Bartole, A.; Greenberg, S.; Resendes, R.; Coombs, N.; Safa-Sefat, A.; Greedan, J. E; Stoever, H. D. H.; Ozin, G. A.; Manners, I. *J. Am. Chem. Soc.* **2002**, *124*, 12522–12534. (b) McDowell, J. J.; Zacharia, N. S.; Puzzo, D.; Manners, I.; Ozin, G. A. *J. Am. Chem. Soc.*, **2010**, *132*, 3236–3237.

(39) PFS block copolymer micelles formed in selective solvents have previously been shown to be redox active, see: (a) reference 24a; (b) Wang, H.; Wang, X.; Winnik, M. A.; Manners, I. *J. Am. Chem. Soc.* **2008**, *130*, 12921–12930.

(40) Eitouni, H. B.; Balsara, N. P. *J. Am. Chem. Soc.* **2004**, *126*, 7446–7447.

(41) Li, J. K.; Zou, S.; Rider, D. A.; Manners, I.; Walker, G. C. *Adv. Mater.* **2008**, *20*, 1989–1993.

(42) For a brief communication of some of this work see ref 24b.

(43) Péter, M.; Lammertink, R. G. H.; Hempenius, M. A.; Vancso, G. J. *Langmuir* **2005**, *21*, 5115–5123.

(44) (a) Rider, D. A.; Cavicchi, K. A.; Power-Billard, K. N.; Russell, T. P.; Manners, I. *Macromolecules* **2005**, *38*, 6931–6938. (b) Lammertink, R. G. H.; Hempenius, M. A.; Vancso, G. J. *Macromol. Chem. Phys.* **1998**, *199*, 2141–2145.

(45) Eloi, J.-C.; Rider, D. A.; Wang, J.-Y.; Russell, T. P.; Manners, I. *Macromolecules* **2008**, *41*, 9474–9479.

(46) Nguyen, M. T.; Diaz, A. F.; Dement'ev, V. V.; Pannell, K. H. *Chem. Mater.* **1993**, *5*, 1389–1394.

(47) (a) Giannotti, M. I.; Lv, H.; Ma, Y.; Steenvoorden, M. P.; Overweg, A. R.; Roerdink, M.; Hempenius, M. A.; Vancso, G. J. *J. Inorg. Organomet. Polym. Mater.* **2005**, *15*, 527–540. (b) Espada, L.; Pannell, K. H.; Papkov, V.; Leites, L.; Bukalov, S.; Suzdalev, I.; Tanaka, M.; Hayashi, T. *Organometallics* **2002**, *21*, 3758–3761.

(48) Arsenault, A. C.; Míguez, H.; Kitaev, V.; Ozin, G. A.; Manners, I. *Adv. Mater.* **2003**, *15*, 503–507.

(49) Ciminale, F.; Lopez, L.; Farinola, G. M.; Sportelli, S. *Tetrahedron Lett.* **2001**, *42*, 5685–5687.

(50) Identified by a color change from dark blue to pale pink.

(51) Masson, G.; Beyer, P.; Cyr, P. W.; Lough, A. J.; Manners, I. *Macromolecules* **2006**, *39*, 3720–3730.

(52) Schmidt, W.; Steckhan, E. *Chem. Ber.* **1980**, *113*, 577–585.

(53) Wesley, R. D.; Dreiss, C. A.; Cosgrove, T.; Armes, S. P.; Thompson, L.; Baines, F. L.; Billingham, N. C. *Langmuir* **2005**, *21*, 4856–4861.

(54) Connelly, N. G.; Geiger, W. E. *Chem. Rev.* **1996**, *96*, 877–910.

(55) $[SbCl_6]^-$ has 2.24 times the volume of $[SbF_6]^-$ based on Sb^V in an octahedral environment. The respective ionic radii for Sb, F and Cl are 74×10^{-12}, 119×10^{-12}, and 167×10^{-12} m. Assuming a radius of the sphere, that contains the octahedral anion, being equal to the radius of Sb plus the diameter of the halogen, $[SbCl_6]^-$ has a volume of 2.85×10^{-28} m^3 and $[SbF_6]^-$ 1.27×10^{-28} m^3.

(56) Cao, L.; Manners, I.; Winnik, M. A. *Macromolecules* **2002**, *35*, 8258–8260.
(57) Massey, J. A.; Temple, K.; Cao, L.; Rharbi, Y.; Raez, J.; Winnik, M. A.; Manners, I. *J. Am. Chem. Soc.* **2000**, *122*, 11577–11584.
(58) Wang, X.; Guerin, G.; Wang, H.; Wang, Y.; Manners, I.; Winnik, M. A. *Science* **2007**, *317*, 644–647.
(59) Gädt, T.; Ieong, N. S.; Cambridge, G.; Winnik, M. A.; Manners, I. *Nat. Mater.* **2009**, *8*, 144–150.
(60) Gilroy, J. B.; Gädt, T.; Whittell, G. R.; Chabanne, L.; Mitchels, J. M.; Richardson, R. M.; Winnik., M. A.; Manners, I. *Nature Chem.* **2010**, *2*, 566–570.
(61) For studies on the crystallization of PFDMS see: (a) Rasburn, J.; Petersen, R.; Jahr, T.; Rulkens, R.; Manners, I.; Vancso, G. J. *Chem. Mater.* **1995**, *7*, 871–877. (b) Lammertink, R. G. H.; Hempenius, M. A.; Manners, I.; Vancso, G. J. *Macromolecules* **1998**, *31*, 795–800. (c) Papkov, V. S.; Gerasimov, M. V.; Dubovik, I. I.; Sharma, S.; Dementiev, V. V.; Pannell, K. H. *Macromolecules* **2000**, *33*, 7107–7115. (d) Xu, J.; Ma, Y.; Hu, W.; Rehahn, M.; Reiter, G. *Nat. Mater.* **2009**, *8*, 348–353. (e) Xu, J.; Bellas, V.; Jungnickel, B.; Stühn, B.; Rehahn, M. *Macromol. Chem. Phys.* **2010**, *211*, 1261–1271.
(62) (a) Korczagin, I.; Lammertink, R. G. H.; Hempenius, M. A.; Golze, S.; Vancso, G. J. *Adv. Polym. Sci.* **2006**, *200*, 91–117. (b) Cao, L.; Massey, J. A.; Winnik, M. A.; Manners, I.; Riethmüller, S.; Banhart, F.; Spatz, J. P.; Möller, M. *Adv. Funct. Mater.* **2003**, *13*, 271–276.
(63) Shen, L.; Wang, H.; Guerin, G.; Wu, C.; Manners, I.; Winnik, M. A. *Macromolecules* **2008**, *41*, 4380–4389.